Ion beam synthesis of cubic-SiC layer on Si(111) substrate

R. L. Maltez, R. M. de Oliveira, R. M. S. dos Reis, and H. Boudinov

Citation: Journal of Applied Physics **100**, 063504 (2006); doi: 10.1063/1.2344813
View online: http://dx.doi.org/10.1063/1.2344813
View Table of Contents: http://scitation.aip.org/content/aip/journal/jap/100/6?ver=pdfcov
Published by the AIP Publishing

Ion beam synthesis of cubic-SiC layer on Si(111) substrate

R. L. Maltez,[a] R. M. de Oliveira, R. M. S. dos Reis, and H. Boudinov
Instituto de Física, UFRGS, C.P. 15051, 91501-970 Porto Alegre, Rio Grande do Sul, Brazil

(Received 28 December 2005; accepted 27 June 2006; published online 20 September 2006)

We have investigated SiC layers produced by ion beam synthesis on Si(111) substrates using different procedures. Bare Si(111) and SiO_2/Si(111) structures were implanted with carbon at 40 keV up to a fluence of 4×10^{17} cm^{-2} at a temperature of 600 °C. Postimplantation annealing was carried out at 1250 °C for 2 h in pure O_2 or Ar (with 1% of O_2). A SiC layer was synthesized for all the procedures involving annealing under Ar. However, for the samples annealed under pure O_2 flux, only that employing implantation into the bare Si(111) resulted in SiC synthesis. Rutherford backscattering spectrometry shows that, after annealing, the stoichiometric composition is obtained. Transmission electron microscopy measurements demonstrate the synthesis of cubic-SiC layers that are completely epitaxial to the Si(111) substrate. However, there is a high density of nanometric twins, stacking faults, and also narrow amorphous inclusions of laminar shape between the crystalline regions. The procedure based on high temperature implantation through a SiO_2 cap, etching the cap off, 1250 °C postimplantation annealing under Ar ambient (with 1% of O_2), and final etching has shown advantages from the point of view of surface flatness and increased layer thickness, keeping the same layer epitaxy and accurate composition. © *2006 American Institute of Physics*. [DOI: 10.1063/1.2344813]

I. INTRODUCTION

SiC semiconductor is well known by its high thermal and chemical stabilities,[1] which are attractive for high power operation, and also by its large band gap (2.2–2.9 eV), which is appropriate for light emission in the green to blue range.[1] However, the light emitting recombination efficiency[2] for SiC is only about 0.02% (indirect band gap); it can be partially compensated for by the capability to work at higher current levels.

SiC can be used as a substrate of choice for GaN heteroepitaxial growth. GaN semiconductor also has high thermal and chemical stabilities with the additional advantage of being a direct band gap semiconductor. Blue InGaN-based lasers on GaN substrates, for example, are available on the market,[3] where special growing techniques[3,4] have to be employed to obtain a GaN material with low density of threshold dislocations. These dislocations are formed as a result of a large misfit between GaN and sapphire basal lattice parameters (a_{GaN}=0.3189 nm and a_{Sap}=0.4758 nm, respectively). SiC is offering a better lattice matching (a_{SiC}=0.3076 nm) to GaN. An important additional advantage in having SiC as substrate is that its thermal conductivity is about four times higher than the GaN one, while the sapphire thermal conductivity is about four times lower.[1] But in practice SiC is not the preferred substrate for GaN growing, probably due to its smaller wafer size and higher cost.

The possibility of obtaining epitaxial SiC on Si can bring some technological benefits, and it is an active research field.[5–12] Some straightforward advantages are cheaper and larger substrate area, Si–SiC device integration, Si–GaN device integration through a SiC intermediate layer, and thermal dissipation improvement of GaN devices, since Si thermal conductivity is almost the same as the GaN. In this work, we are investigating the possibility of obtaining a SiC layer on Si(111) by using ion implantation technique, which is deeply employed in Si processing steps. Some authors have attempted such synthesis,[5–8] almost all of them into Si(111), since SiC and GaN can be also found in the hexagonal symmetry.[1] Lindner,[8] however, implanted C into Si(100) and demonstrated the synthesis of cubic-SiC eptiaxial to Si(100) matrix. Ristic *et al.*[7] used multiple C implantations into Si(111) at very high total doses (2.6×10^{18} C/cm^2), followed by reactive ion etching on the surface. Ito *et al.*[5] and Yamamoto *et al.*[6] employed a procedure similar to Lindner,[8] but they used Si(111) wafers. Yamamoto *et al.*[6] performed postimplantation annealing under O_2 atmosphere and a subsequent etching of the oxidized layer. By performing refelection high-energy electron diffraction (RHEED) pattern on the etched surface, they verified the presence of a single crystalline cubic-SiC layer. Finally, they used this layer as substrate for GaN growing, which has demonstrated half of the tensile stress, as compared with GaN layer grown on AlN/Si substrates.[13] However, they reported a relatively rough surface.

In this work, we have explored different procedures for SiC ion beam synthesis. Carbon was implanted into bare and oxidized Si(111). High temperature postimplantation annealing was performed either in O_2 or in an inert atmosphere with 1% O_2. Characterization of the synthesized structures was done by transmission electron microscopy (TEM) and Rutherford backscattering spectrometry (RBS)/channeling measurements, in order to understand the consequences of each treatment and to identify the layer of increased structural quality. We have observed important differences on the final structure depending on the performed procedure.

[a]Electronic mail: maltez@if.ufrgs.br

II. EXPERIMENTAL DETAILS

Bare Si($\bar{1}11$) and SiO_2/Si($\bar{1}11$) structures (110 nm thick thermally grown SiO_2) were implanted with 40 keV of carbon up to a fluence of 4×10^{17} cm^{-2} at a temperature of 600 °C. We will name these samples bare Si and SiO_2/Si, respectively. All carbon implantations have been done using a 500 kV ion implanter with a current density of about 0.5 $\mu A/cm^2$.

The carbon low dose depth distribution simulated by TRIM (Ref. 14) program is a Gaussian-like profile with an average projected range of about 110 nm and a full width at half maximum (FWHM) of about 78 nm. If this low dose depth profile was valid for high dose ion implantation, we would have almost pure carbon at the depth of the peak concentration. However, as observed in some works,[6,8] sample temperature and depth extension dynamically redistribute the implanted atoms, and a wider profile with a composition closer to the Si:C ratio of 1:1 may be obtained.

A number of Si samples implanted with SiO_2 cap had their oxide removed by HF etching prior to annealing, giving rise to a third distinct set. All samples were submitted to postimplantation annealing at 1250 °C for 2 h. Two distinct annealing ambients were employed: a reactive one, where samples of each set were annealed under a flux of high purity and dry O_2 gas, and an almost inert one, where samples of each set were annealed under a flux consisting of a mixture of 99% Ar and 1% O_2. In the end, we had an ensemble of six different approaches to be investigated. The annealing had two main purposes: to improve the quality of the synthesized SiC layer, and especially for the bare Si samples, to oxidize the Si surface. Finally, in order to remove the oxide and reveal the buried SiC layer, all the annealed samples were etched in $HF:H_2O$ (1:2) solution.

The structural information was obtained using the JEOL JEM 2010 transmission electron microscope of the Center for Electron Microscopy at UFRGS, operated at 200 kV of acceleration voltage. Cross-sectional specimens were prepared by mechanical polishing and dimpling, followed by ion polishing at shallow angles (~6°). We have also performed RBS measurements, under random incidence and also aligned to the [$\bar{1}11$] sample direction (channeling normal to the surface). These measurements were carried out with a 1.2 MeV He^+ beam produced by a 3 MV tandem accelerator.

III. RESULTS AND DISCUSSIONS

A. As-implanted bare Si and SiO_2/Si samples

The synthesis of SiC during the implantation is demonstrated by selected area diffraction (SAD) under TEM measurements. In these measurements, we have selected the implanted region as the one to generate the diffraction pattern (our smallest TEM aperture has a diameter typically twice the thickness of the formed SiC layer; thus, Si matrix spots are always expected). Figure 1 shows a SAD pattern ([110] zone axis) corresponding to the as-implanted SiO_2/Si sample, but there is no substantial difference between this diffraction pattern and that from the bare Si sample. In Fig. 1, we can identify always two spots for the same **g** vector, where the outer spots are consistent with the synthesis of a cubic-SiC structure. The measured lattice parameter for the SiC structure was about 0.44 nm, which is in good agreement with the cubic phase of SiC (Refs. 1 and 15) (a_{SiC} =0.435 nm). Other main feature observed in all diffraction patterns is that the synthesized SiC structures are completely epitaxial to the Si matrix, as if we had a continuous layer or SiC grains with the same orientation as the Si substrate.

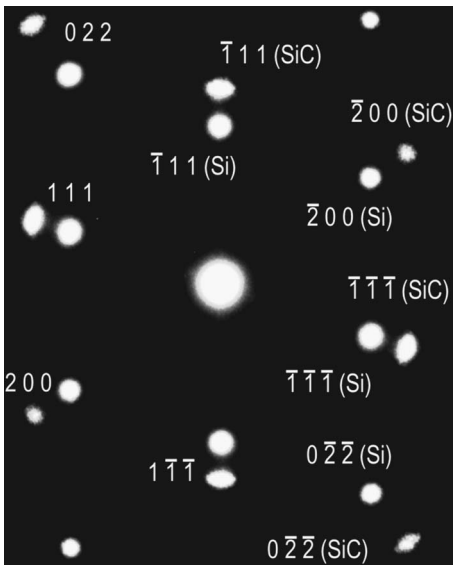

FIG. 1. SAD pattern for the as-implanted SiO_2/Si sample taken from an area including the implanted region. The outer spots for distinct **g** vectors demonstrate the synthesis of a cubic-SiC structure epitaxial to the Si(111) substrate (inner spots).

Figures 2(a)–2(d) are cross-sectional TEM micrographs from the as-implanted samples, where the surface is at their top (indicated by the arrow heads). Figs. 2(a) and 2(b) were taken from the bare Si sample, while Figs. 2(c) and 2(d) are from the SiO_2/Si one. All micrographs were taken close to a two-beam condition for the planes ($\bar{1}11$) of the SiC structure. The left column images [(a) and (c)] are bright field (BF $\bar{1}11$), while the right column images are their respective dark field (DF $\bar{1}11$) ones. From Fig. 2(a) (bare implanted Si) we can observe the carbon-rich region extending to about 145 nm from the sample surface, which is followed by an end-of-range defect region up to about 270 nm. Under DF $\bar{1}11$ condition for the SiC crystals [Fig. 2(b)], we can observe a denser white band with some dispersed white dots at its extremes. This white region is mainly located in a depth range between about 55 and 145 nm from the sample surface.

Regarding the samples implanted with a SiO_2 cap on their surfaces [Figs. 2(c) and 2(d)], we can promptly observe the amorphous SiO_2 layer extending from the surface to about 70 nm [Fig. 2(c)], which means that about 40 nm of the superficial SiO_2 was sputtered off during the implantation procedure. In addition, the implanted carbon region is fairly the same as that of the bare sample [Figs. 2(a) and 2(b)], i.e., it also extends to the depth of about 140 nm from the sample surface. In particular, the corresponding DF $\bar{1}11$ condition

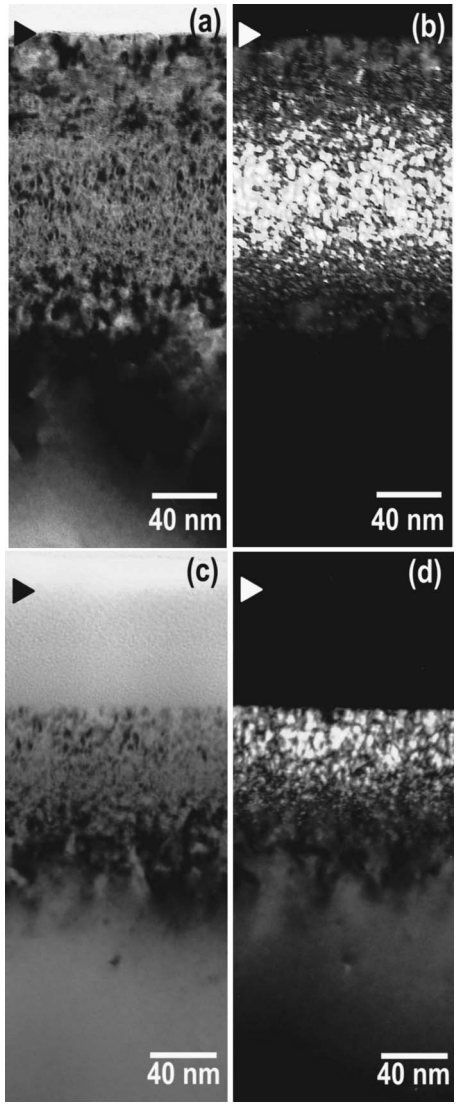

FIG. 2. [(a)–(d)] Cross-sectional TEM micrographs from the as-implanted samples (sample surface is indicated by the arrow heads). (a) and (b) were taken from the bare Si(111) sample, while (c) and (d) from the SiO_2/Si(111) one. All micrographs were taken close to a two-beam condition for the planes $(\bar{1}11)$ of the SiC structure. The left column images [(a) and (c)] are bright field (BF $\bar{1}11$), while the right column images are their respective dark field (DF $\bar{1}11$) ones.

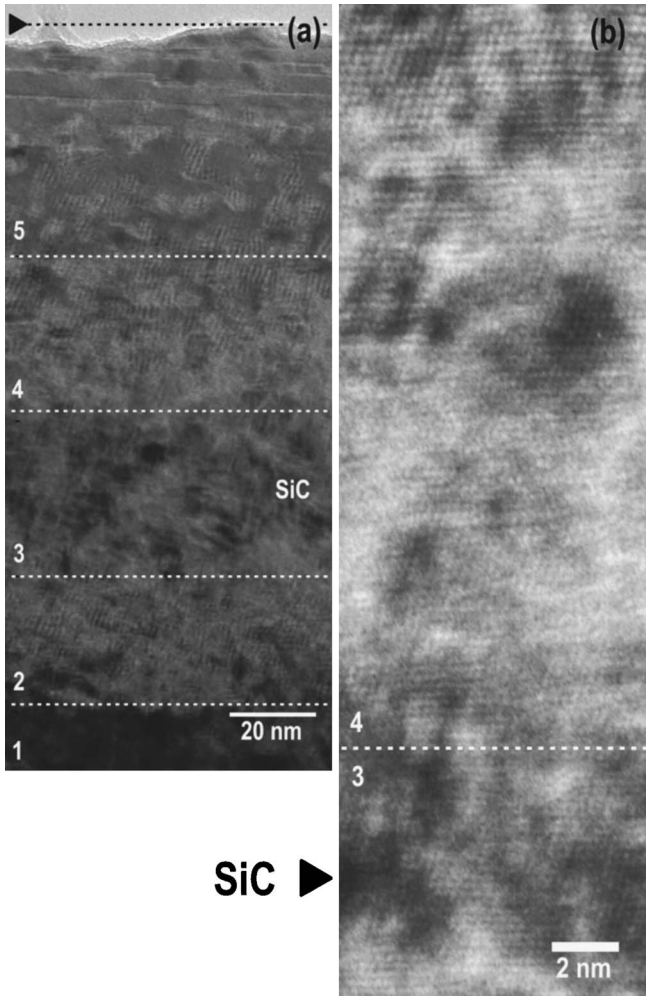

FIG. 3. [(a) and (b)] Cross-sectional HRTEM micrographs for the bare Si(111) as implanted sample taken along [110] zone axis. (a) Low-magnified view of the implanted area. Labels (from inside to outside the sample): 1—Si(111) substrate; 2—SiC/Si(111) inner interface; 3—SiC layer; 4—Si(111)/SiC outer interface; and 5—Si close to surface with isolated SiC precipitates. (b) Magnified HRTEM image showing the boundary between layers 4 [Si(111)/SiC outer interface] and 3 (SiC layer).

[Fig. 2(d)] shows that the SiO_2/Si interface is approximately located at the beginning of the white band shown in Fig. 2(b).

RBS measurements were also carried out on these samples (not shown). Simulation of RBS spectra reveals synthesized layers with distinct compositions (estimated stoichiometric error is about ±0.01): $Si_{0.56}C_{0.44}$ for the bare Si implanted sample, while the SiO_2/Si sample is at the correct composition $Si_{0.5}C_{0.5}$. However, both substrates were placed together on the implantation sample holder and the distinct compositions cannot be explained by differences in the implantation procedure. One possible explanation for obtaining a layer less rich in carbon for the bare Si substrate could be an occasional channeling of the C beam (even though the sample holder was intentionally tilted by some degrees). This effect is less pronounced (or inexistent) for the oxidized sample due to a dechanneling component offered by the superficial amorphous layer.

TEM DF images, as shown in Figs. 2(b) and 2(d), would not suggest synthesis of a continuous single crystalline SiC layer. But, according to Fig. 1, a cubic-SiC layer with the same orientation as the Si substrate has been formed. A better understanding of the formed structure can be obtained from the TEM analysis of Fig. 3(a), which was taken from the bare Si implanted sample. Figure 3(a) is a high resolution TEM (HRTEM) image taken along the [110] zone axis, but shown at low magnification. It is evident that a layered structure is formed, already at the as-implanted state, since there is an alternation of lighter and darker regions as a function of the depth (dashed lines were inserted to aid the eyes). Such layers were labeled with numbers 1–5, where number 1 is the deepest region (silicon matrix), while region 5 is the closest layer to the surface. The presence of Moirè patterns in some layers is clear in Fig. 3(a). In our case, Moirè patterns are a consequence of the overlap between SiC and Si crystal struc-

tures, which have an epitaxial orientation but distinct lattice parameters. They can reveal the presence of either SiC precipitates in Si, or Si precipitates in SiC.

Region 5 corresponds to a region with few implanted carbon atoms. It begins at the sample surface and extends down to about 55 nm. This is a region where some isolated SiC precipitates are found (Moirè patterns) and no amorphous region was detected in HRTEM images. Layers 4–2 form the region between the depths of ~55 and ~155 nm, which correspond to the carbon-rich region as mentioned before [white region on Fig. 2(b)]. Analysis of HRTEM images is coherent with the following: (i) layer 4 is the Si/SiC interface closer to the surface; (ii) layer 3 is a continuous but highly disordered SiC layer with a thickness of 35 nm (the Moirè patterns that could help to identify Si precipitates are not present), and (iii) layer 2 is the deeper SiC/Si interface.

Figure 3(b) is a HRTEM image showing the boundary between layers 4 (SiC interface) and 3 (SiC layer). The upper side of this figure is close to region 5, and shows lattice contrast combined with Moiré pattern, i.e., crystalline region with coexistence of Si and SiC crystals at the same depth. The bottom part of this figure is the synthesized SiC layer (layer 3). Such region is highly disordered, and the lattice image of the SiC could not be perfectly defined. However, the calculated diffraction pattern (Fourier tranform exclusively done over the image area of layer 3) has exactly reproduced the SiC spots of the experimental diffraction pattern, i.e., outer spots as shown in Fig. 1. The presence of disordered and/or amorphous SiC or Si regions in this layer would generate dark regions under DF images, and, in this sense, the white band observed under DF [Figs. 2(b) and 2(d)] could not be a continuous bright region. However, while the existence of amorphous clusters of Si is possible for the bare Si case, it is improbable for the sample with SiO_2/Si, which has a stoichiometric SiC layer.

The central area of Fig. 3(b) (at the Si/SiC interface, region 4) clearly demonstrates the existence of amorphous regions closer to the SiC layer. Similar condition is also observed at layer 2 (the deeper SiC/Si interface, not shown). However, in this case, the amorphous and Moiré patterns seem to be more homogeneously distributed along the interface.

B. Bare Si samples annealed in O_2 and Ar/1% O_2

Figures 4(a)–4(c) are results from bare Si sample after postimplantation annealing at 1250 °C for 2 h under dry O_2 gas flux, after removal of the thermally grown SiO_2 layer of the sample surface. Figure 4(a) shows RBS measurements under random incidence (open circles) and also aligned (full circles) along the $[\bar{1}11]$ sample direction. As we can see, the channeled spectrum shows a poor minimum yield (χ_{min} =85%) for the SiC layer. However, some improvement has been obtained in relation to the as-implanted case (not shown), where no channeling was verified for the synthesized SiC layer (χ_{min}=100%). RBS simulation of the random spectra reveals a synthesized layer with a composition of $Si_{0.49}C_{0.51}$ (the estimated error is about ±0.01) and a thickness of 30 nm. Then, the annealing under O_2 flux has promoted changes in the SiC layer composition from Si-rich ($Si_{0.56}C_{0.44}$) to stoichiometric SiC.

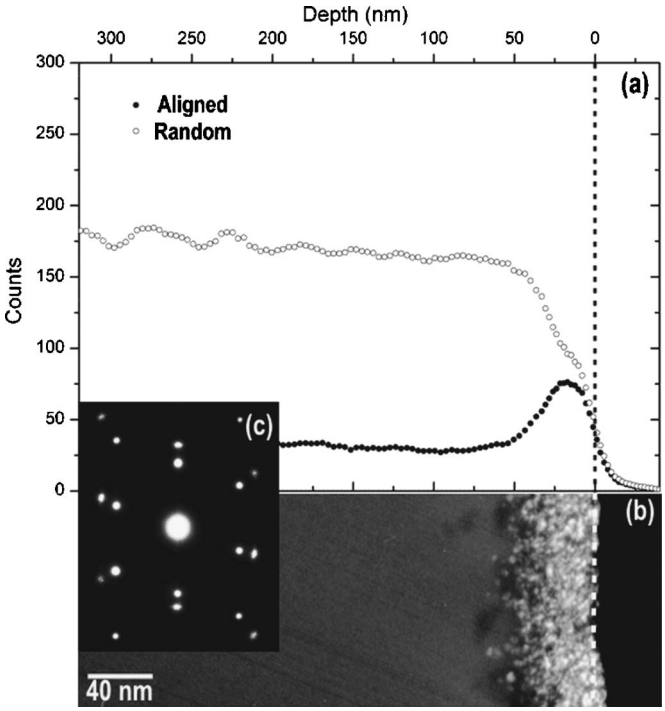

FIG. 4. [(a)–(c)] Results from bare Si sample after annealing at 1250 °C for 2 h in dry O_2. (a) RBS spectra under random incidence (open circles) and aligned (full circles) to the $[\bar{1}11]$ sample direction. (b) Cross-sectional TEM micrograph (DF 200 for the SiC structure) with the surface at the right side (dashed lines). SiC layer is the white region. (c) Inset showing the measured SAD pattern: It demonstrates a cubic-SiC structure epitaxial to the Si matrix.

Figure 4(b) is a cross-sectional TEM micrograph, where the surface is at the right side and the dashed line indicates the surface position. This is a dark field image close to a two-beam condition for the (200) planes of SiC structure (DF 200), and thus the SiC layer is imaged as the white region. As we can see in Fig. 4(b), the SiC layer has a thickness of about 30 nm, and it is now at the sample surface, which is undulated with maximum amplitude of about 6 nm. A layer thickness of 30 nm is close to the thickness of about 35 nm associated with layer 3 (SiC layer) of Fig. 3(a) (HRTEM of the as-implanted material). It indicates that the annealing temperature for 2 h was high enough to completely oxidize layers 4 and 5 (layer 4—Si/SiC interface closer to the surface, and layer 5—dispersed SiC precipitates embedded in Si). Apparently, some SiC material from region 3 was converted into SiO_2. The inset in Fig. 4(c) corresponds to a SAD pattern of the SiC layer. This pattern is basically the same as shown in Fig. 1 and demonstrates the synthesized SiC layer having a cubic-SiC structure and being completely epitaxial to the Si matrix.

Figures 5(a)–5(c) are results from bare Si samples after postimplantation annealing at 1250 °C for 2 h under Ar with 1% O_2. The samples were etched in HF solution in order to remove the thermally grown thin SiO_2 layer from the surface. Figure 5(a) presents RBS measurements under random incidence (open circles) and also aligned (full circles) along

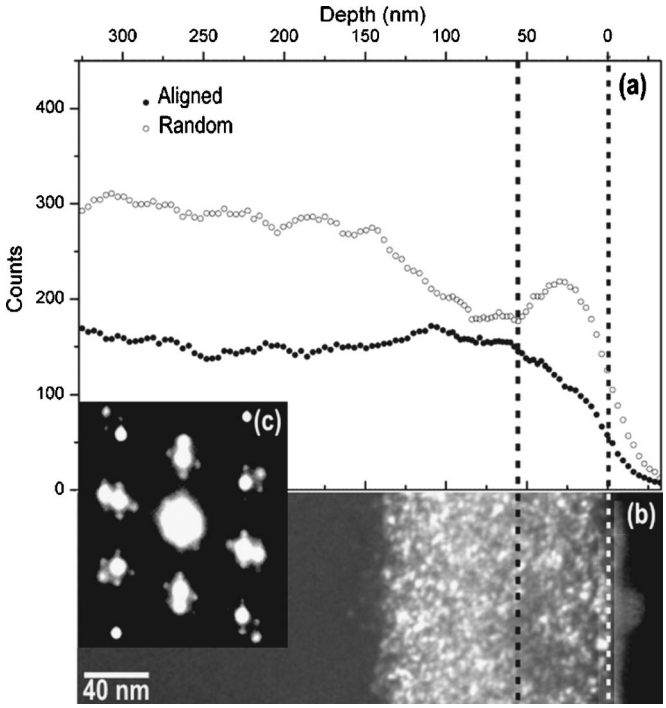

FIG. 5. [(a)–(c)] Results from bare Si sample after annealing at 1250 °C for 2 h in Ar with 1% O_2. (a) RBS spectra under random incidence (open circles) and aligned (full circles) to the $[\bar{1}11]$ sample direction. (b) Cross-sectional TEM micrograph (DF 200 for the SiC structure) with the surface at the right side (first dashed line from the right). SiC layer is still buried in this sample (second dashed line is at about the interface). (c) SAD pattern: Pronounced double diffracted extra spots over the regular SAD pattern.

the $[\bar{1}11]$ sample direction. Figure 5(b) is a cross-sectional TEM micrograph under DF 200 condition for the SiC structure, where the surface is at the right side and the dashed line indicates the surface position. The inset in Fig. 5(c) corresponds to a SAD pattern of the corresponding SiC layer.

Figures 5(a) and 5(b) are both consistent with the formation of a layered structure where the SiC layer is still buried in the sample, while the near surface layer is formed by SiC precipitates imbedded into Si. RBS simulation (not shown) performed at the random spectrum of Fig. 5(a) has evidenced that the buried layer has an almost correct SiC composition (it has changed from $Si_{0.56}C_{0.44}$, before annealing, to $Si_{0.53}C_{0.47}$). The composition of the near surface layer is, however, much richer in Si ($Si_{0.77}C_{0.23}$). For this reason, the channeled spectrum in Fig. 5(a) (full circles) shows a χ_{min} that gradually increases from about 30% (at surface) to 85% at the SiC depth. This demonstrates the coexistence of Si and SiC crystals at the same depth (in the near surface layer), i.e., there is a more effective ion beam channeling in Si crystals.

The observed SAD pattern [Fig. 5(c)] demonstrates pronounced extra spots in addition to the cubic-SiC and Si diffraction spots [compared to Fig. 1 or 4(c)]. These extra spots are from the double diffraction of the electron beam due to the coexistence of Si and SiC crystals at the same depth in the near surface layer. Additional hypothesis for extra spots were also considered: (i) inclusions of SiC hexagonal phases and (ii) inclusions of twinned precipitates. The first option was disregarded by software calculation of corresponding diffraction patterns. For the second, we have investigated twin {111} planes for both Si and SiC structures. These mirror planes would generate extra spot distribution similar to some of the experimental spots. However, the resulting pattern clearly did not match the experimental pattern. Considering extra spots from double diffraction phenomenon (i.e., a first diffraction in Si followed by re-diffraction in SiC, or vice versa), a perfect match between theoretical and experimental patterns was obtained. This effect is mainly due to the near surface layer, which consists of Si with SiC precipitates.

C. SiO_2/Si samples annealed in O_2

RBS/channelling measurements (not shown) do not demonstrate any synthesis of SiC layer for those samples implanted through SiO_2 cap and submitted to annealing at 1250 °C for 2 h under O_2 flux. The remaining material, after etching in HF solution, is just the substrate silicon with an excellent crystal quality, i.e., $\chi_{min}=5\%$. This result is observed for samples annealed with or without the SiO_2 cap. It indicates a SiC oxidation rate not negligible for the as-implanted material.

D. SiO_2/Si samples annealed in Ar/1% O_2

A SiC layer is synthesized for samples implanted through the SiO_2 cap and annealed at 1250 °C for 2 h (with or without SiO_2 cap layer during the annealing) under a flux of Ar with 1% O_2.

Figures 6(a)–6(c) are HRTEM images under [110] zone axis of the sample annealed without the SiO_2 cap. Figure 6(a) reveals a SiC thickness of 45 nm (sample surface is marked with an arrow head at the top of the figure). The SiC thickness increases to 55 nm when the sample is annealed with the SiO_2 cap (not shown). Both thicknesses are much larger than the one obtained for bare Si sample under O_2 flux (35 nm). In addition, the present procedure produces smoother surfaces. Simulation of the RBS spectra (not shown) shows that the stoichiometric composition was reached in both cases.

The SiC layer is formed by crystalline regions, or grains, welded by laminar amorphous regions in between [Fig. 6(a)]. Since the layer is at the stoichiometric composition, such amorphous or very disordered regions are also made of SiC material. These observations can explain why continuous layers of SiC show a granular type contrast under usual BF and DF TEM images. The crystalline regions are all epitaxial to the Si(111) substrate, as demonstrated by SAD patterns. HRTEM measurements show that the near surface area (down to 15 nm below the surface) is more disordered for samples annealed with the SiO_2 cap.

A high density of twins and stacking faults can be observed in Fig. 6(a), in the SiC layer. The faults and twin planes are both on {111} planes. For example, in Fig. 6(a), the arrow head *B* marks the position of a defect we have interpreted as a very narrow twin inclusion between two $(\bar{1}11)$ twin planes. A magnified view of this area is shown in Fig. 6(b). Since these twins are very narrow, their corresponding extra twin spots, in the SAD pattern, could not be observed.

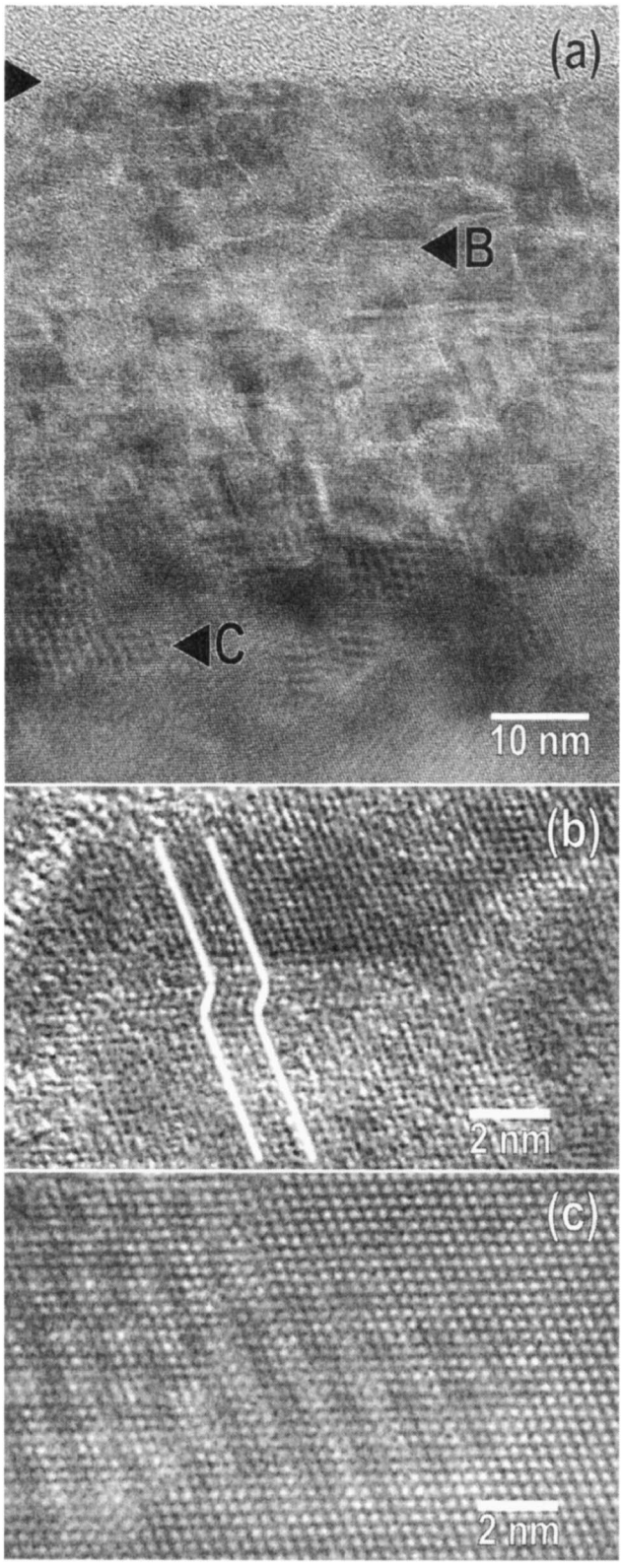

FIG. 6. [(a)–(c)] Cross-sectional HRTEM micrographs for the SiO_2/Si implanted sample, and annealed without the SiO_2 cap, taken along [110] zone axis. (a) Low-magnified view of the synthesized SiC layer: lighter and upper region with the surface position marked by the upper arrow head. A high density of amorphous zones, twins, and stacking faults can be observed. (b) Magnified HRTEM image of the area indicated by the arrow head B showing a nanometer-scale twin inclusion between two $(\bar{1}11)$ twin planes. (c) Magnified HRTEM image of the area indicated by the arrow head C showing the typical Moirè pattern (SiC precipitate inclusion) on the substrate Si(111).

Figure 6(c) is a magnified view of the area pointed with the arrowhead *C* in Fig. 6(a). As can be seen, this is an area in the Si substrate, just at the end of the SiC/Si interface. It shows the typical Moirè pattern observed in our samples. Also, the crystalline planes are now much better defined than they were at the SiC layer [compared to Fig. 6(b)]. This is another indication of the noticeable difference between the crystal quality of the substrate and the synthesized SiC layer. These observations clarify why we do not observe ion beam channeling for aligned RBS spectra of SiC layers, although SiC layer keeps an epitaxial alignment to Si(111) substrate, as revealed by SAD patterns.

IV. CONCLUSIONS

We have shown SiC layers produced by ion beam synthesis on Si(111) substrates, aiming to expose the SiC layer to the sample surface. A SiC layer was synthesized in all samples annealed under Ar flux (with 1% of O_2). When the annealing was carried out under pure O_2, the synthesis was obtained only for the bare Si sample. For those samples implanted through a SiO_2 cap, the SiC layer was not obtained after annealing in O_2 ambient.

Flat SiC layers on the sample surface were obtained for SiO_2 capped samples after annealing under Ar and further etching. They were also thicker than the one obtained for the bare Si sample. However, postimplantation annealing performed with the SiO_2 cap resulted in more disordered surfaces (down to 15 nm below the surface). RBS measurements demonstrated that, after annealing, a correct Si:C ratio of 1:1 was obtained for almost all the cases. Some channeling ($\chi_{min}=85\%$) was observed at the SiC layer obtained from bare Si implanted samples, but none from SiO_2/Si ones. It suggests that C implantation into bare Si produces samples with a better crystal quality as compared to the ones implanted with a SiO_2 cap (but the flatness of the surface is much better for the latter). TEM measurements demonstrated that the synthesized layer is cubic-SiC and is epitaxial to the Si(111) substrate. However, it has a high density of extended defects (twins and stacking faults) and also narrow inclusions of amorphous phase (laminarlike) between the crystalline regions. The procedure based on high temperature implantation through a SiO_2 cap, etching the cap off, 1250 °C postimplantation annealing under Ar ambient (with 1% of O_2), and final etching has shown advantages from the point of view of surface flatness and increased thickness. It also demonstrates the same epitaxial alignment and stoichiometric composition as observed for bare Si samples annealed in pure O_2. Work is in progress to improve the crystalline quality of the synthesized SiC layer, however, at this point, it could be used as a substrate for different material growing processes.

ACKNOWLEDGMENTS

The authors gratefully acknowledge financial support from FAPERGS and CNPq.

[1]H. Morkoç, S. Strite, G. B. Gao, M. E. Lin, B. Sverdlov, and M. Burns, J. Appl. Phys. **76**, 1363 (1994).

[2]J. A. Edmond, H. S. Kong, and C. H. Carter, Jr., Physica B **185**, 453 (1993).
[3]S. Nakamura, M. Senoh, S. Nagahama, N. Iwasa, T. Matsushita, and T. Mukai, Appl. Phys. Lett. **76**, 22 (2000); S. Nakamura *et al.*, *ibid.* **72**, 2014 (1998).
[4]A. Usui, H. Sunakawa, A. Sakai, and A. A. Yamaguchi, Jpn. J. Appl. Phys., Part 2 **36**, L899 (1997).
[5]Y. Ito, T. Yamauchi, A. Yamamoto, M. Sasase, S. Nishio, K. Yasuda, and Y. Ishigami, Appl. Surf. Sci. **238**, 159 (2004).
[6]A. Yamamoto, T. Yamauchi, T. Tanikawa, M. Sasase, B. K. Ghosh, A. Hashimoto, and Y. Ito, J. Cryst. Growth **261**, 266 (2004).
[7]J. Ristic *et al.*, Mater. Sci. Eng., B **93**, 172 (2002).
[8]J. K. N. Lindner, Nucl. Instrum. Methods Phys. Res. B **178**, 44 (2001).
[9]D. Wang, Y. Hiroyama, M. Tamura, M. Ichikawa, and S. Yoshida, Appl. Phys. Lett. **77**, 1846 (2000); **76**, 1683 (2000).
[10]C. W. Liu, A. St. Amour, J. C. Sturm, Y. R. J. Lacroix, M. L. W. Thewalt, C. W. Magee, and D. Eaglesham, J. Appl. Phys. **80**, 3043 (1996).
[11]A. J. Steckl, J. Devrajan, C. Tran, and R. A. Stall, Appl. Phys. Lett. **69**, 2264 (1996).
[12]C. A. Zorman, A. J. Fleischman, A. S. Dewa, M. Mehregany, C. Jacob, S. Nishino, and P. Pirouz, J. Appl. Phys. **78**, 5136 (1995).
[13]D. G. Zhao, S. J. Xu, M. H. Xie, S. Y. Tong, and H. Yang, Appl. Phys. Lett. **83**, 677 (2003).
[14]J. F. Ziegler, J. P. Biersack, and U. Littmark, *The Stopping and Range of Ions in Solids* (Pergamon, Oxford, 1985), Vol. 1.
[15]R. W. G. Wyckoff, *Crystal Structures*, 2nd ed. (Interscience, New York, 1963).